

# Modelling system integration of a micro solar Organic Rankine Cycle plant into a residential building

Alessia Arteconi<sup>a,b</sup>, Luca Del Zotto<sup>a</sup>, Roberto Tascioni<sup>a,c</sup>, Luca Cioccolanti<sup>a\*</sup>

<sup>a</sup>Università Telematica e-Campus, Via Isimbardi 10, 22060 - Novedrate, CO, Italy.

<sup>b</sup>Dipartimento di Ingegneria Industriale e Scienze Matematiche, Università Politecnica delle Marche, via Brecce Bianche 1, Ancona 60131, Italy

<sup>c</sup>DIAEE, Sapienza Università di Roma, via Eudossiana 18, Rome 00184, Italy

\* Corresponding author: e-mail: luca.cioccolanti@uniecampus.it Phone: +39 071 2204127

## Abstract

In the present energy scenario and considering the high share on global energy demand of buildings, small and micro-scale combined heat and power units powered by solar energy are considered a suitable solution for many industrial and civil applications, such as residential buildings. In this work a micro solar Organic Rankine Cycle plant is analysed. The system consists of a concentrated Linear Fresnel Reflectors solar field coupled with a phase change material thermal energy storage tank and a 2kWe/18kWth Organic Rankine Cycle system. In this work the integration of such system with a building is investigated in detail by means of a dynamic simulation model. In particular their interaction is analysed to assess its impact on the Organic Rankine Cycle electric and thermal performance. Furthermore, the building heating system optimization is evaluated aiming at minimizing the energy operational costs of the building. Results show the convenience of the proposed micro solar combined heat and power system when it works in trigeneration configuration. They highlight also that the operational strategy and the dynamic energy demand of the building affect the Organic Rankine Cycle performance and 26% higher electricity production is obtained with the integrated plant-building model compared to the plant without building integration. Regarding the building parameters design, they affect the energy cost only if they are varied simultaneously and their optimal set-up can allow up to 9% energy cost savings, thanks to a better exploitation of the available energy produced by the micro solar plant.

**Keywords:** micro combined cooling heat and power plant; concentrated solar power; ORC system; renewable energy; energy storage; system integration; residential applications.

## Nomenclature

A	area of the primary collectors [m <sup>2</sup> ]
A <sub>o</sub>	outer surface area of the heat exchanger node [m <sup>2</sup> ]
A <sub>i</sub>	inner surface area of the heat exchanger node [m <sup>2</sup> ]
ACH	Air Changes per Hour
a <sub>l</sub> , b <sub>l</sub>	coefficients of heat losses
a <sub>t</sub> , b <sub>t</sub> , c <sub>t</sub>	coefficients of turbine isentropic efficiency
C <sub>el</sub>	electricity price [€/kWh <sub>e</sub> ]
C <sub>NG</sub>	natural gas price [€/GJ]
C <sub>p,c</sub>	specific heat of the cooling water [kJ/(kg·K)]
C <sub>p,fluid</sub>	specific heat of the fluid [kJ/(kg·K)]
C <sub>r</sub>	capacitance flow rate ratio
C <sub>tot</sub>	total energy operational cost [€]
Cost <sub>var</sub>	energy cost variation [%]
COV <sub>DHW</sub>	coverage of Domestic Hot Water thermal energy demand [%]
COV <sub>el</sub>	coverage of electric energy demand [%]
COV <sub>SC</sub>	coverage of space cooling thermal energy demand [%]
COV <sub>SH</sub>	coverage of space heating thermal energy demand [%]
COV <sub>th</sub>	coverage of total thermal energy demand [%]
COV <sub>tot</sub>	coverage of total energy demand [%]
CHP	Combined Heat and Power
d <sub>i</sub>	inner diameter of the tube [m]
d <sub>coil</sub>	diameter of the coil [m]
DHW	Domestic Hot Water
DNI	Direct Normal Irradiation [kW/m <sup>2</sup> ]
E <sub>aux</sub>	electricity consumption of the absorption chiller auxiliaries [kWh <sub>e</sub> ]
E <sub>boiler</sub>	total energy produced by boiler [kWh <sub>t</sub> ]
E <sub>chiller</sub>	electricity consumption of the back-up chiller [kWh <sub>e</sub> ]
E <sub>el,ORC</sub>	ORC electricity production [kWh <sub>e</sub> ]
E <sub>th,ORC</sub>	ORC thermal energy production [kWh <sub>t</sub> ]
E <sub>pump</sub>	electricity consumption of pump [kWh <sub>e</sub> ]
f	function of PCM and oil temperature properties
f <sub>FullLoadCapacity</sub>	fraction of the device's full load capacity during operation under current conditions
f <sub>NominalCapacity</sub>	fraction of the device's nominal capacity during operation under current conditions
h <sub>air</sub>	enthalpy of the air [J/kg]
h <sub>o</sub>	outer surface heat transfer coefficient [J/(m <sup>2</sup> ·K)]
h <sub>i</sub>	inner surface heat transfer coefficient [J/(m <sup>2</sup> ·K)]
h <sub>sat</sub>	saturation enthalpy of the air [J/kg]
IAM	Incident Angle Modifier
k <sub>c</sub>	compensation curve coefficient in winter season
LFR	Linear Fresnel Reflector
$\dot{m}_{air}$	mass flow rate of the air [kg/s]
$\dot{m}_{air,design}$	mass flow rate of the air at design conditions [kg/s]
$\dot{m}_c$	mass flow rate of the cooling water [kg/s]
$\dot{m}_f$	mass flow rate of the organic fluid [kg/s]
$\dot{m}_{fluid}$	mass flow rate of the fluid flowing through the boiler [kg/s]
n	number of identical coiled tubes of the heat exchanger
NTU	Number of Transfer Units
NU <sub>hx</sub>	Nusselt number
OM	Operation Mode
ORC	Organic Rankine Cycle
P <sub>el,ORC</sub>	electric power produced by the ORC [kW <sub>e</sub> ]
P <sub>in,ORC</sub>	inlet thermal power to the ORC [kW <sub>t</sub> ]
P <sub>th,ORC</sub>	outlet thermal power from the ORC [kW <sub>t</sub> ]
P <sub>LFR,out</sub>	outlet thermal power from the LFR [kW <sub>t</sub> ]
P <sub>tank,loss</sub>	thermal power loss through the TES envelope [kW <sub>t</sub> ]
P <sub>th,net</sub>	useful thermal power delivered to the building [kW <sub>t</sub> ]

$P_{waste}$	thermal power dissipated by the air cooler [kW <sub>t</sub> ]
PES	Primary Energy Savings
PCM	Phase Change Material
$PE_{var}$	Primary Energy variation [%]
$Pr_{hx}$	Prandtl number
PTC	Parabolic Trough Collectors
PV	Photovoltaic
$Q_{conv, surf}$	convective gain from surfaces [kW <sub>t</sub> ]
$Q_{inf}$	infiltration gains [kW <sub>t</sub> ]
$Q_{int, gains}$	internal gains [kW <sub>t</sub> ]
$Q_{loss}$	heat losses at the receiver [kW <sub>t</sub> ]
$Q_{node}$	heat exchanged at the air node [kW <sub>t</sub> ]
$Q_{PCM}$	heat exchanged by the PCM [kW <sub>t</sub> ]
$Q_{solar, rad}$	solar gains [kW <sub>t</sub> ]
$Q_{vent}$	ventilation gains [kW <sub>t</sub> ]
$\dot{Q}_{fluid}$	energy delivered to the liquid stream through the boiler [kW]
$\dot{Q}_{fluid, design}$	energy delivered to the liquid stream through the coils at design conditions [kW]
Ra	Rayleigh number
$R_w$	tube wall resistance [m <sup>2</sup> K/W]
$Re_{hx}$	Reynolds number
RES	Renewable Energy Sources
SC	Space Cooling
SH	Space Heating
t	time
TES	Thermal Energy Storage
$T_{abs}$	absorber temperature [°C]
$T_{air}$	outside ambient air temperature [°C]
$T_{in, cond}$	inlet temperature of the cooling water at the condenser [°C]
$T_{out, cond}$	outlet temperature of the cooling water at the condenser [°C]
$T_{in, fluid}$	inlet temperature of the fluid [°C]
$T_{out, fluid}$	outlet temperature of the fluid [°C]
$T_{oil}$	temperature of the diathermic oil [°C]
$T_{ORC, off}$	lower bound temperature set-point of the PCM storage tank [°C]
$T_{ORC, on}$	upper bound temperature set-point of the PCM storage tank [°C]
$T_{PCM, av}$	average temperature of the PCM storage tank [°C]
$T_{supply}$	temperature of the water supplied to the underfloor heating system [°C]
U	thermal transmittance [W/(m <sup>2</sup> ·K)]
UA	overall heat transfer coefficient of the immersed heat exchanger [W/K]

#### Greek symbols

$\alpha$	solar elevation angle
$\epsilon$	efficiency of the heat exchanger
$\lambda$	enthalpy ratio
$\eta_{boiler}$	boiler efficiency
$\eta_{el}$	electric conversion efficiency
$\eta_m$	mechanical efficiency
$\eta_{opt}$	optical efficiency
$\eta_{opt, max}$	maximum optical efficiency
$\eta_{el, ORC}$	ORC electric efficiency
$\eta_t$	turbine isentropic efficiency
$\eta_{th, ORC}$	ORC thermal efficiency
$\eta_{th, int}$	overall thermal efficiency of the plant integrated with the building
$\eta_{rec}$	receiver efficiency
$\sigma$	solar azimuthal angle
$\theta$	solar incident angle
$\Delta h_e$	actual specific enthalpy difference across the expander [kJ/(kg K)]
$\Delta h_p$	actual specific enthalpy difference across the pump [kJ/(kg K)]

$\Delta T_{PCM}$	temperature difference between the PCM and the heat transfer medium [°C]
$\Delta t_{int-timestep}$	time interval of the internal time step [s]

## 1. Introduction

In Europe the building sector accounts for about 40% of the final energy consumption and 36% of CO<sub>2</sub> emissions [1]. In 2010 the Energy Performance of Buildings Directive and in 2012 the Energy Efficiency Directive have set the specifications for high energy performance buildings and for the adoption of energy efficiency measures within the EU. Among energy efficient technologies, combined heat and power (CHP) systems allow the reduction of primary energy consumptions and, as a consequence, limit CO<sub>2</sub> emissions. For this reason the European Directive 2004/8/EC [2] has encouraged European countries to develop combined heat and power systems and has supported their use in different sectors. Indeed, wherever thermal and electrical demands are simultaneous, CHP systems offer potential benefits.

Going towards a decentralised energy production, small and micro-scale CHP units proved to be suitable for many industrial and civil applications, such as residential buildings. Although micro-CHP systems have a very interesting potential in households to curb CO<sub>2</sub> emissions [3], their adoption has been limited so far, because of the economic feasibility. Indeed, micro-CHP actual convenience strongly depends on the scenario in which they are expected to operate. Hence, a proper design of micro-CHP systems for heating supply to residential buildings is of paramount importance for their economic success [4]. Users energy demand, electricity and fuel tariffs as well as adequate incentives are the main factors affecting their profitability.

In 2015, CHP fuel mix in Europe was mainly based on fossil fuels, whilst renewable sources accounted for about 20.6% [5]. In order to meet the challenging targets set by the Paris Agreement, an increasing share of renewable energy sources (RES) was introduced in the last years in the power generation mix, supported by existing regulation and subsidies [6]. Furthermore, distributed generation technologies using renewable energy allow to increase the security of supply in developed countries and to provide access to safe, reliable, affordable and clean energy in rural areas of developing countries. Despite internal combustion engines are the most well-established prime movers for small and micro-scale CHP applications [7] and are already available in the market, some issues still need to be solved, such as the introduction of renewable fuels for their more environmentally-friendly operation. Hence, Martinez et al. [8] conducted an extensive literature review on micro-CHP systems based on renewable energies with particular focus on solar based technologies. Micro solar CHP units, indeed, are considered effective means to provide clean, efficient and secure energy to the building sector. At present, the most used technology for renewable thermal energy production at residential level is represented by evacuated tube solar panels, because of their ease of installation and absence of tracking mechanisms [9]. However, the use of medium and high temperature solar technologies in buildings is preferable for cogeneration applications and they can be competitive with evacuated tubes if the involved systems are properly designed [10]. In particular, Organic Rankine Cycle (ORC) systems are considered as one of the most common and competitive technologies to efficiently convert the solar energy into power [11]. Therefore, many researchers are paying attention on the development and optimization of small-

scale ORC systems. Furthermore, special interest exists for ORC coupled with different solar technologies. For example, Freeman et al. [12] evaluated the electrical performance of a domestic solar ORC using evacuated flat-plate solar collectors and investigated different solutions to optimize its operation in the UK climate. Baccioli et al. [13] carried out a dynamic simulation of a small-scale solar ORC power unit with rotary volumetric expander using compound parabolic collectors for different Italian locations. The control strategy proposed by the authors allowed operating without any storage system. Manfrida et al. [14], instead, first developed a mathematical model of a thermal energy storage system made of phase change material and then evaluated its application in a solar powered ORC using parabolic trough collectors. The analysis shown that the proposed plant was able to produce electricity for almost 80% of the investigated period with a weekly average overall efficiency of 3.9% (solar-to-electricity). Tacconi et al. [15] carried out laboratory and field tests of a prototypal solar ORC (< 10 kWe) coupled with a 100 m<sup>2</sup> parabolic trough collectors (PTC) solar field obtaining a gross electrical efficiency of the ORC unit up to 8%.

In order to properly assess the actual potential of solar ORC in residential applications, their integration into the building needs to be accurately addressed. So far, most of the works in literature about micro solar CHP systems based on ORC units focused on the optimization of the different subsystems or of the whole plant, neglecting their exact interaction with the building. For example, Ramos et al. [16] performed a complete system optimisation considering the design parameters both of two different solar collector arrays and of a non-regenerative sub-critical ORC unit to be used in a domestic environment. In particular, the authors found that a 60 m<sup>2</sup> evacuated-tube solar field coupled with an ORC engine is able to deliver an electrical and thermal output of 3'605 kWh/year and 13'175 kWh/year respectively for the city of Athens with a levelised cost of energy close to that of PV systems. Calise et al. [17] carried out a dynamic simulation in TRNSYS of a 6 kWe ORC system coupled with a 73.5 m<sup>2</sup> solar field, consisting of novel flat-plate evacuated collectors and an auxiliary gas-fired heater to provide additional thermal energy to the ORC in case it is needed. The yearly output electrical and thermal energy by the ORC system was found to be 4'300 kWh and 41'200 kWh, respectively, with an additional heat input from the gas-fired burner of only 3'000 kWh. The issue of micro-CHP integration in building is, indeed, a relevant topic and it is confirmed by the fact that several studies in literature dealt with the coupling of ~~other~~ different micro-CHP technologies, rather than solar, into buildings. For example, Fubara et al. [18] proposed a modelling framework to capture the impact of the adoption of solid oxide fuel cells, Stirling engines and internal combustion engines micro-CHP systems on the total primary energy usage in both generation and distribution by using as case study four different sizes of UK houses. ~~Di Marcoberardino et al. [19] evaluated the energy and economic balance of a 10 kWe Proton Exchange Membrane Fuel Cell cogeneration unit in a residential application using an in-house software. In particular, they assessed the system profitability in a distributed generation scenario with varying loads and natural gas and electricity prices.~~ Rosato et al. [20], instead, investigated in TRNSYS the energetic, economic and environmental performance of a 6 kWe micro-CHP unit based on internal combustion engine technology in a multi-family house in Naples. ~~In another paper, Rosato et al. [21] performed numerical simulations in four different Italian cities to estimate the influence of climatic conditions and operational strategies on the performance of the 6 kWe natural~~

gas-fuelled internal combustion engine cogeneration unit. In particular, they found that even in case of thermal load following logic the primary energy savings (PES) achieved by the cogeneration unit differs significantly with location. Furthermore, the same authors [22] assessed the performance of the same cogeneration unit feeding an electric air-cooled vapour compression chiller for cooling purposes in Italian residential applications. Whatever the city under investigation, the proposed system was able to reduce the primary energy consumption with respect to the conventional energy production even though the PES was always negative from April to October. Also Fong and Lee [23] conducted, by means of TRNSYS, a year-round evaluation of trigeneration systems based on internal combustion engine technology subject to climatic conditions. In this case, prime movers under investigation were coupled with single-effect absorption chillers to satisfy the electrical, thermal and cooling energy demands of a 30-storey office. Four Asian cities with close longitudes and different latitudes were considered. The analysis revealed that a continental climate with cold winter and hot summer is favourable to trigeneration, whilst a temperate climate results in a low energy-saving potential for such trigeneration systems. Therefore, renewable energy and solar technologies in particular could be of paramount importance to extend the energy profitability of cogeneration and trigeneration systems also in temperate climate zones. Hence, Rodriguez et al. [24] analysed the performance of several design configurations of a hybrid solar thermal/PV/micro-CHP system, composed of a natural gas internal combustion engine as micro-CHP unit, integrated into a building in different locations of Spain. Also Yang and Zhai [25] presented a simulation work of a solar hybrid cooling and combined heat and power plant in three building prototypes across seven climate zones. The buildings energy demand is obtained with models in Energy Plus and then used to optimize the design schemes of the plant, represented in a separate model in Matlab. Instead, Martinez et al. [26] performed a numerical investigation on the performance of a micro solar CHP system consisting of a 46.5 m<sup>2</sup> PTC solar field, a single-cylinder steam engine working according to a Hirn cycle and an additional boiler integrated into a two-floors house in Chambéry. The simulation analysis developed in TRNSYS revealed that the volume of the water tank between the plant and the building has a huge impact on the operating hours of the plant. Garcia-Saez et al. [27] evaluated the economic and technical feasibility of solar ORC systems to cover the domestic hot water and electricity demand of residential buildings. They highlighted that the profitability is strictly related to the coverage of the energy demand. The authors claimed the need to develop dynamic simulation models to properly assess the interaction between demand and production. As regards ORC based cogeneration/trigeneration units, Zhang et al. [28] conducted different simulations of a prototype scale PTC-ORC system with a power output of 200 kW<sub>e</sub> and coupled with a single effect absorption chiller. In particular, the authors focused on different time-scale analyses to evaluate the functionality and the dynamic of the integrated technologies to provide electrical, thermal and cooling power to a baseline office building. According to mid-term simulations, the annual production of the optimized system under investigation was equivalent to 79.9%, 95.9% and 53.3% of the cooling, heating and electrical energy demand of the building. However, the mutual interactions between the solar ORC system and the building is not analysed in detail, but heating and cooling curves are used. Such aspect cannot be neglected for a fair evaluation of the performance of micro solar ORC system. Indeed, Pereira et al. [29] highlighted how micro ORC

systems in residential applications have the ability to face highly variable thermal demand loads with a short response time, nevertheless, to the best of the authors' knowledge, just a few works in literature about solar ORC systems have already dealt with this topic taking into account the daily system dynamics and the mutual influence between energy demand and supply. Wang et al. [30] showed the potential of the integration of a combined heat and power unit and a concentrating solar power plant with buildings integrated with phase change materials. In particular they optimized the energy demand scheduling in order to maximize the energy efficiency of the system, which refers to large scale applications and relies on solar tower as concentrated solar power technology. In a previous paper Arteconi et al. [31], analysed the potential of a micro solar ORC system to provide space heating and domestic hot water in residential dwellings in different European countries. In this work a detailed evaluation at building level of the energy deployment of an innovative micro solar ORC plant in residential dwellings is performed, but the influence on the production unit operation is neglected. The innovative micro solar ORC was presented in [32], where its operation and energy performance were also discussed. The plant is composed of a small-scale 2kWe Organic Rankine Cycle system coupled with a concentrated solar Linear Fresnel Reflector (LFR) plant and a phase change material (PCM) thermal storage system equipped with reversible heat pipes, as proposed in the Innova MicroSolar EU project [33] led by Northumbria University [34]. The analysis highlighted that the plant is able to achieve a significant number of operating hours during the year with pretty good electric and thermal efficiencies. Moreover, the electric and thermal energy production is adequate to partially satisfy the energy demand of several dwellings. However, in order to better evaluate the useful energy production from the plant, which can effectively cover the thermal and electric demand of a building, a detailed dynamic simulation model for the integrated system (plant-building) was here developed, because the interaction in dynamic operation of energy demand and supply ~~has a paramount importance on~~ significantly affects the overall system performance. Purpose of the analysis is both understanding the influence of the integration on the ORC unit efficiency and also assessing the useful energy that can be recovered for the building needs. Furthermore an optimization of the integrated system is proposed. Hence, the main novelties of the work rely on: (i) the assessment of the performance of a novel micro-CHP system based on LFR solar field by means of an integrated model including both the dynamic behaviour of the plant and of the building; (ii) the comparison of the overall system performance in case of using an integrated simulation model or a fixed ORC condensing temperature (i.e. a given load curve for the building energy demand) to quantify the impact of the real operation strategy. In particular the latter aspect is not retrieved in other literature works, as highlighted in Table 1 where the main features of the relevant literature studies analysed in the state of the art review are summarized. It is evident that there is a lot of research interest in the field, however different technologies are described in the listed papers, with different research targets and research methodologies.

The paper is organized as follows: in Section 2 the methodology of the analysis is presented, in Section 3 the system and simulation model are described, while in Section 4 the main results are discussed. Eventually Section 5 summarizes the main findings of the work.

Table 1. Summary of the main aspects of reported literature studies about solar CHP systems for buildings.

Reference	CHP plant	Size	Building representation	Objective of the study
[12]	evacuated flat-plate solar collectors; ORC	Domestic size (electric annual average power about 100 W; solar collector area 15 m <sup>2</sup> )	-	Optimal working fluid selection and configuration
[13]	compound parabolic collectors; ORC	N.A.	-	Performance analysis
[14]	parabolic trough collectors; latent thermal storage; ORC	solar collector area 2600 m <sup>2</sup>	-	Role of the latent thermal storage
[15]	parabolic trough collectors; ORC	<10 kW <sub>el</sub> ; solar collector area 100 m <sup>2</sup>	-	Performance analysis in lab
[16]	flat-plate and evacuated-tube solar field; ORC	solar collector area 60 m <sup>2</sup>	-	Performance analysis
[17]	flat-plate evacuated collectors, ORC	6 kW <sub>el</sub> ; solar collector area 73.5 m <sup>2</sup>	-	Performance analysis
[25]	hybrid system: PV and solar thermal panels; gas fueled CHP plant	Hospitals, hotels and offices application	load curve (obtained with a separated Energy Plus model)	Optimal design and performance analysis
[26]	parabolic trough collector; steam engine	Domestic application; solar collector area 46.5 m <sup>2</sup> , dwelling of 4 users in Chambéry (France)	integrated TRNSYS model	Role of the storage tank
[27]	flat collectors; ORC and reversible heat pump	solar collector area 40 m <sup>2</sup> , dwelling of 4 users in Sanlucar (Spain)	load curve	Economic and performance analysis
[28]	parabolic trough collector; ORC; absorption chiller	200 kW <sub>el</sub> , office building, western region of China	load curve	Performance analysis
[30]	solar tower; absorption chiller	up to 40 MW, 5000 households in China	RC model	Economic and performance analysis

[32]	linear Fresnel reflector solar collector; ORC	2 kWel; solar collector area 146 m <sup>2</sup>	-	Performance analysis
present work	linear Fresnel reflector solar collector; ORC; absorption chiller	2 kWel; solar collector area 146 m <sup>2</sup> , 4 dwellings in Spain	integrated TRNSYS model	Performance comparison in case of simulation model with or without integrated building

## 2. Methods

In this paper the integration of a micro solar ORC plant with a residential building is investigated. The analysis is performed by means of a dynamic simulation model that represents both the plant and the building. First the ORC production is assessed considering an ideal thermal energy demand: the final user can use all the energy produced by the ORC and the condenser works at fixed temperature depending on the chosen configuration (i.e. cogeneration or trigeneration mode). Then the integrated operation of the ORC and the building is considered, taking into account the influence of the building demand on the ORC condensing temperature and thus on the ORC thermal and electric energy production and efficiency. Indeed the thermal interaction between the two systems is relevant for the performance of the ORC unit and a detailed analysis is required, while the corresponding electric energy produced is only compared with an assumed average electricity demand for the final user [35]. Eventually the heating and cooling system configuration in the building is optimized, in order to minimize the operational costs and the necessary final user energy demand to reduce the amount of wasted ORC thermal energy production.

The plant is supposed to be located in Lerida (41° 37' 0" N, 0° 38' 0" E), very close to the Spanish city where the real prototype of the Innova Microsolar project has been built. The direct normal irradiance for this location is 2429 kWh/m<sup>2</sup> and the global horizontal irradiance 1882 kWh/m<sup>2</sup>. It is a place with typically cold winter and hot summer. A dynamic simulation model was set up using TRNSYS [36] to model the plant and the coupled building. The main components of the plants were included in the model in TRNSYS and ad-hoc subroutines were written in Matlab [37] to represent the LFR solar field, the micro ORC plant and the PCM thermal energy storage tank equipped with reversible heat pipes. The weather data file was obtained from Energy+ database [38] and a simulation time step of 10 minutes was assumed. In Figure 1 the integrated plant-building system is represented and described in detail in the next Sections.

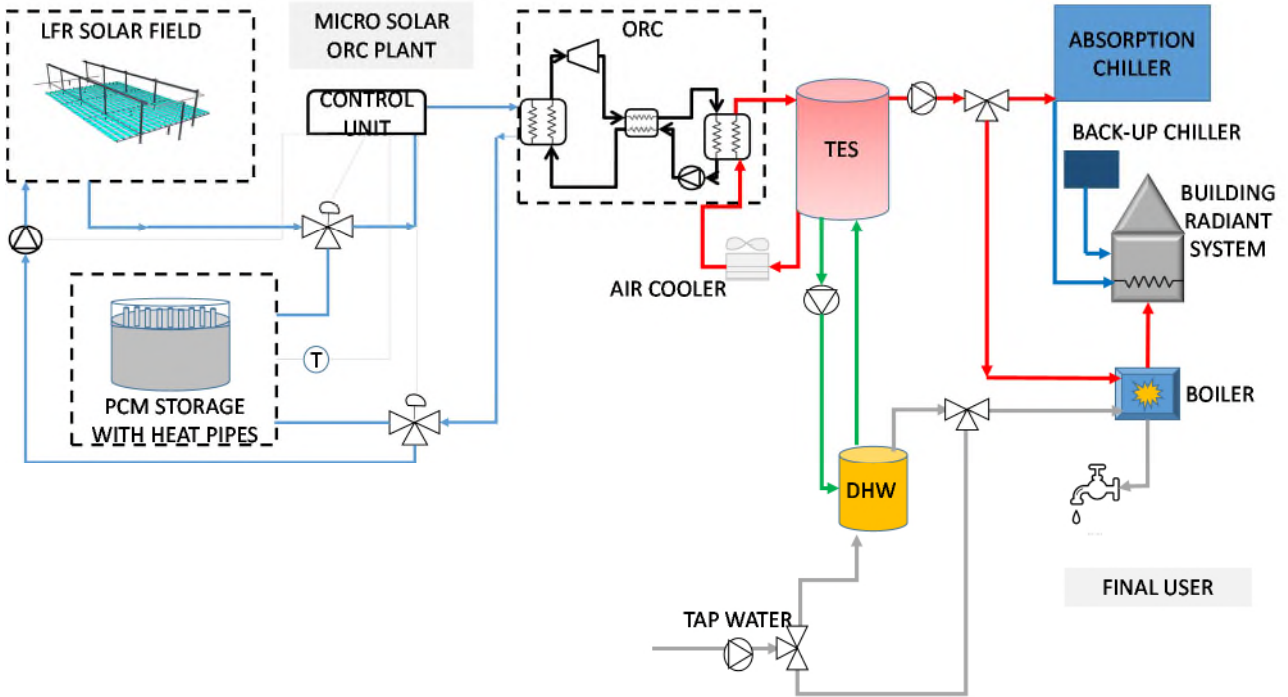


Figure 1. Integrated plant-building system schematics: the main components of the micro-solar Organic Ranking Cycle and the final user's heating and cooling devices are illustrated.

### 3. System description

#### 3.1 Micro solar ORC plant

The plant consists of: (i) a concentrated linear Fresnel reflector solar field producing heat at temperatures in the range 250-280°C; (ii) a 2kWe/18kWt Organic Rankine Cycle plant; (iii) an advanced PCM thermal storage tank equipped with reversible heat pipes (Figure 1). It was conceived by the consortium of several Universities and industrial organizations under the EU funded InnoVa MicroSolar Project [33] and it was sized to supply small residential or commercial buildings. With more detail, the solar field has a net mirror surface area of about 146 m<sup>2</sup> and the receiver consists of evacuated tube collectors placed at about 3.5 m from the ground. The LFR solar field is able to achieve a peak thermal power output of about 80 kWt at nominal operating conditions (DNI equal to 900 W/m<sup>2</sup>), as declared by the manufacturing company [39]. In the model, the performance of the LFR solar field has been assessed in terms of its optical efficiency under quasi-steady state conditions. It can be expressed as in Eq. 1:

$$\eta_{opt} = \eta_{opt, max}(\theta=0) \cdot IAM(\alpha, \sigma) \quad (1)$$

where  $\theta$  is the solar incident angle,  $\alpha$  the solar elevation angle and  $\sigma$  the azimuthal angle and  $\eta_{opt, max}$  the maximum optical efficiency of the LFR reached when the incident angle is zero. The IAM is the Incident Angle Modifier and its values have been provided for the considered collector by the manufacturing company ELIANTO [39] at different solar elevation and azimuth. Therefore, taking

into account the thermal losses of the absorber tubes  $Q_{loss}$  the collected thermal energy of the LFR can be calculated as follows:

$$P_{LFR,out} = A \cdot DNI \cdot \cos(\theta) \cdot \eta_{opt} \cdot \eta_{rec} - Q_{loss} \quad (2)$$

where,  $A$  is the area of the primary collectors,  $\cos(\theta)$  the cosine of the solar incident angle and  $\eta_{rec}$  the receiver efficiency.

The oil flow rate in the solar field is adjusted in order to keep the oil temperature at 210°C when the solar field supplies the ORC, thus assuring a good electric conversion efficiency of the ORC unit or at 10°C more than the average PCM storage temperature in case the solar field supplies the storage. The ORC unit was designed by ENOGIA [40] and it operates accordingly to a regenerative cycle using NOVEC 649 as working fluid [41]. On the basis of the operational conditions, the working fluid is heated up in the evaporator using directly the energy collected by the LFR solar field or the thermal energy stored by the storage tank. The fluid expands in an axial turbine to theoretically achieve a gross electric power production of about 2 kWe and a conversion efficiency of about 10 %. In particular, the electric power output from the ORC is:

$$P_{el,ORC} = \dot{m}_f \cdot [\eta_m \cdot \eta_{el} \cdot \Delta h_e - \Delta h_p / (\eta_m \cdot \eta_{el})] \quad (3)$$

with  $\dot{m}_f$  the organic fluid flow rate,  $\eta_m$  the mechanical efficiency,  $\eta_{el}$  the electric efficiency,  $\Delta h_e$  and  $\Delta h_p$  the actual specific enthalpy difference across the expander and the pump based on the following assumptions:

- a minimum superheating at the evaporator of 5 °C;
- no subcooling at the outlet of the condenser;
- an organic working fluid flow rate of 0.21 kg/s at nominal operating conditions, which is adjusted, at every time step, in order to maintain the minimum superheating at the evaporator outlet;
- a generator electric efficiency equal to 0.9 and a mechanical efficiency of 0.95;
- a constant overall heat transfer efficiency of the heat exchangers.

The thermal power output from the ORC unit is evaluated as:

$$P_{th,ORC} = \dot{m}_c \cdot c_{p,c} \cdot (T_{out,cond} - T_{in,cond}) \quad (4)$$

where  $\dot{m}_c$  is the cooling water flow rate,  $c_{p,c}$  the specific heat of the cooling water and  $T_{out,cond}$  and  $T_{in,cond}$  the outlet and inlet temperatures of the cooling water at the condenser. The thermal energy produced by the ORC is delivered to a thermal energy storage (TES) represented by a thermally stratified water tank (represented with Type 156 in TRNSYS, see Figure 1), which decouples the energy production and demand from the final user, as better explained later on. In case the TES is fully charged, a back-up air cooler (modelled with Type 511 in TRNSYS) is switched on to cool the water return temperature to the condenser (outlet water temperature set-point at 40°C).

The ORC thermal and electric efficiencies are defined respectively as:

$$\eta_{th,ORC} = \frac{P_{th,ORC}}{P_{in,ORC}} \quad (5)$$

$$\eta_{el,ORC} = \frac{P_{el,ORC}}{P_{in,ORC}} \quad (6)$$

In order to guarantee 4 hours of ORC unit operation during night time with a nominal input power of 25 kW, an innovative thermal energy storage system is integrated into the plant. This thermal energy storage system, as designed by Northumbria University and Aavid Thermacore [42] and investigated by Lleida University [43], consists of 3.8 tons of nitrate solar salt KNO<sub>3</sub> (40wt. %)/NaNO<sub>3</sub> (60wt. %), whose melting temperature is in the range 216-223°C [44]. Reversible heat pipes, as developed by Aavid Thermacore [42], are adopted to enhance the heat transfer both from the solar field to the storage tank and from the storage tank to the ORC unit. The PCM storage tank is modelled according to the guidelines of the IEA Task 32 report on advanced storage concepts [45], where a detailed description of Type 185 is provided. The model is based on the following main assumptions: (i) material isotropic and isothermal in each internal time-step; (ii) no hysteresis and subcooling effects; and (iii) charging and discharging not simultaneous. The presence of heat pipes is modelled by both limiting the maximum power exchanged to 40 kW and fixing a minimum temperature difference between the oil and the PCM equal to 5°C.

Hence, the temperature variation of the PCM due to the heat exchanged is given by:

$$\Delta T_{PCM(t+1)} = \Delta T_{PCM(t)} \cdot e^{-[\Delta t_{int-timestep} \cdot f]} \quad (7)$$

where  $f$  is a function of both PCM and oil thermal properties [45]. Then, from the temperature variation of the PCM, it is possible to calculate the heat exchanged as:

$$Q_{PCM(t+1)} = \int_t^{t+1} Q_{PCM(t)} \cdot dt \quad (8)$$

The operation mode of the plant depends on the solar radiation and the state of charge of the PCM storage. The diathermic oil from the solar field flows to the PCM storage and/or directly to the ORC depending on its temperature and on the amount of power collected at the receiver. On the contrary, when the power produced by the solar field is low or zero and the average PCM storage temperature is within a given operating range ( $T_{ORC,on} = 217$  °C and  $T_{ORC,off} = 215$  °C), the thermal energy of the storage can be used to run the ORC unit and assure its operation for a maximum of 4 hours with no sun. Table 2 reports set-points and threshold values of each operation mode (OM) in accordance with the control system developed by S.TRA.TE.G.I.E. srl [46]. In particular, when the LFR supplies directly the ORC (OM1), the target oil temperature to be provided to the ORC for its operation is 210°C. In case there is a surplus of thermal power (>22 kW), the solar field charges also the PCM storage (OM4) and in this case the oil temperature depends on the storage temperature (see Table 2). In case the PCM storage temperature increases too much (>280°C), a defocussing of the LFR mirrors b

egins. Whereas if the LFR has not enough energy to run the ORC (<15 kW), it supplies only the PCM storage and the outlet oil temperature is set at 10°C more than the average storage temperature. When, instead, the PCM storage supplies the ORC, it can provide oil with a temperature in the melting range of the phase change material.

Table 2. Operating conditions for the different operation modes of Innova Microsolar plant model.

Operation Mode	Description	Operating conditions
OM1	LFR supplies ORC	$T_{oil}=210^{\circ}\text{C}$
OM2	System off	-
OM3	LFR supplies PCM storage	$T_{oil}=T_{PCM,av}+10^{\circ}\text{C}$
OM4	LFR supplies PCM storage and ORC	$T_{oil}=210^{\circ}\text{C}$ if $T_{PCM,av}<200^{\circ}\text{C}$ or $T_{oil}=T_{PCM,av}+10^{\circ}\text{C}$
OM5	PCM storage supplies ORC	oil flow rate 0.22 kg/s
OM6	PCM storage and LFR supply ORC	$T_{oil}=210^{\circ}\text{C}$ from LFR and tot oil flow rate 0.22 kg/s

The models of the main components of the plant were tested with available data from manufacturers. Table 3 summarizes the main characteristics of the components represented in the simulation model of the solar ORC plant and integrated building. Further details about the solar ORC plant model can be found in [32].

Table 3. List of models description and mathematical formulation.

Component	Model description	Mathematical formulation
LFR	The model firstly assesses the hourly optical efficiency of the plant and then the thermal power transferred to the oil taking into account the thermal losses at the receiver.	Optical efficiency: Eq. (1); Thermal power output: Eq. (2) Thermal losses: $Q_{loss} = a_l \cdot T_{abs}^4 + b_l \cdot T_{abs}$
PCM tank	The model assesses the heat transferred between the oil flow rate and the PCM, by taking into account the maximum heat transfer rate through the heat pipes	PCM temperature variation: Eq.(7) Heat transferred to PCM: Eq.(8)
ORC	The model evaluates the electric and thermal energy produced by solving the thermodynamic Rankine cycle according to an iterative procedure [47]. The heat transfer rate in the evaporator and condenser heat exchangers is assessed by means of the $\epsilon$ -NTU method The turbine efficiency provided by the manufacturer is used to assess the electric power produced.	Heat exchangers efficiency: $\epsilon = \frac{1 - e^{-NTU \cdot (1-c_r)}}{1 - c_r \cdot e^{-NTU \cdot (1-c_r)}}$ Turbine efficiency: $\eta_t = a_t T^2 + b_t T + c_t$ Electric power: Eq.3 Thermal power: Eq. 4

TES	A thermally stratified water storage tank with an immersed heat exchanger is used (Type 156 [36]). The tank is divided into isothermal temperature nodes, which interact between them for fluid conduction and movement.	Immersed heat exchanger: $\frac{n}{UA} = \frac{1}{h_o A_o} + R_w + \frac{1}{h_i A_i}$ where the outer surface heat transfer coefficient depends on $Nu_D = C \cdot Ra^n$ and the inner surface heat transfer coefficient depends on $Nu_{hx} = 0.023 Re_{hx}^{0.85} Pr_{hx}^{0.4} \left( \frac{d_i}{d_{coil}} \right)^{0.1}$
Building	TRNSYS Type 56 [36] is used to represent the building with active layer for the radiant floor. It is an energy balance model where the air zone heat flux takes into account the thermal exchange by means of convection, infiltration, ventilation, solar radiation and internal gains.	Air zone energy balance: $\dot{Q}_{node} = \dot{Q}_{conv\_surf} + \dot{Q}_{inf} + \dot{Q}_{vent} + \dot{Q}_{int\_gains} + \dot{Q}_{solar\_rad}$
Absorption chiller	TRNSYS Type 107 [36] uses a normalized catalog data lookup approach to model a single-effect absorption chiller.	Heat capacity: $Capacity = f_{FullLoad} Capacity_{Nominal} Capacity_{rated}$
Cooling tower	TRNSYS Type 501 [36] represents a closed loop cooling tower. It assesses the saturated air temperature as the temperature at the air-water interface and assumes it is also the temperature of the outlet fluid.	Saturated air enthalpy: $h_{sat}(T_{fluid,out}) =$ $h_{air}(T_{air,in}) + \frac{\dot{Q}_{fluid,design}}{\dot{m}_{air} \left( 1 - \exp \left[ -\lambda \left( \frac{\dot{m}_{air}}{\dot{m}_{air,design}} \right)^{y-1} \right] \right)}$
Boiler	The model (Type 122 [36]) calculates the energy required to elevate the temperature of the liquid from its inlet value to the setpoint value.	Heat power transferred to the fluid: $\dot{Q}_{fluid} = \dot{m}_{fluid} c_{p,fluid} (T_{out,fluid} - T_{in,fluid})$
Dry cooler	TRNSYS Type 511 [36] is used as dry fluid cooler in which air is blown across coils that contain a hot liquid. The liquid in the coils does not come into direct contact with the air. It is a single-pass, cross-flow heat exchanger represented with the $\epsilon$ -NTU method.	Heat exchangers efficiency: $\epsilon = \frac{1 - e^{-NTU \cdot (1 - c_r)}}{1 - c_r \cdot e^{-NTU \cdot (1 - c_r)}}$

### 3.2 Building specifications

Terraced houses built after 2010 were considered the most suitable final users for this analysis, as assessed in a previous study about potential application of the Innova MicroSolar plant [48]. In particular, a building composed of 4 dwellings was considered because it was demonstrated that it

allows achieving the target set by the Innova Microsolar project of at least 50% of the thermal energy demand coverage and 20% energy costs savings [31]. The considered building was designed on the basis of the specifications for buildings thermal performance in place in Spain [49,50], as reported in Table 4. Each dwelling has a surface of 100 m<sup>2</sup> and a window area of at least 10% of the wall surface. It was assumed about 30 m<sup>2</sup> per person providing an internal gain of 120 W each and a 0.5 ACH (air changes per hour) was modelled. A dynamic simulation model was developed and a schematic of the TRNSYS model is shown in Figure 2.

Table 4. Building thermal specifications (U-values in W/m<sup>2</sup>K).

Country	External walls	Roof	Floor	Windows
Spain	0.74	0.46	0.62	3.1

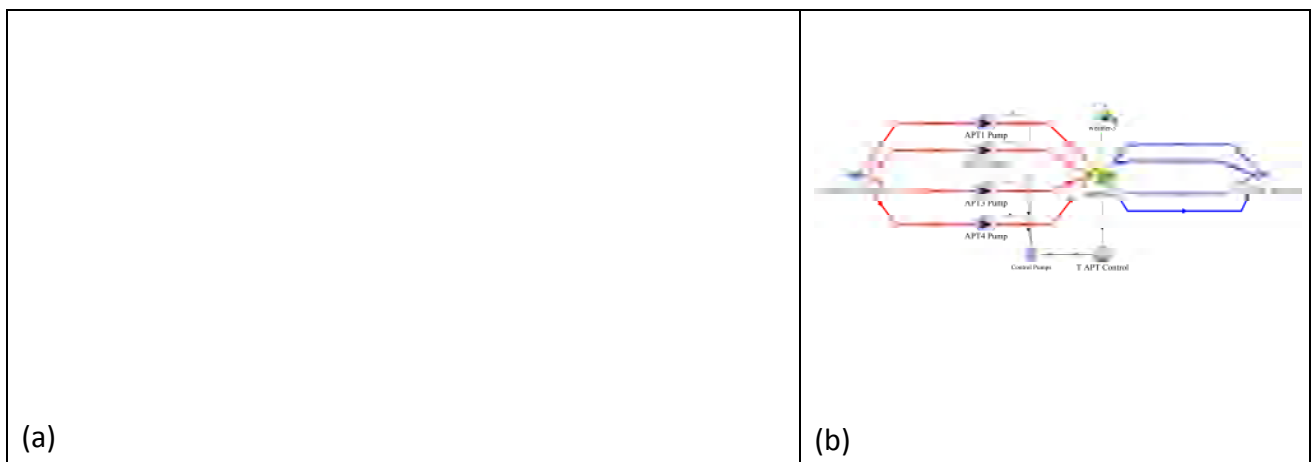


Figure 2. (a)TRNSYS schematics of the integrated model plant-building and (b) detail of the building model with 4 dwellings.

The best available technologies for space heating (SH), space cooling (SC) and domestic hot water (DHW) production were taken into account in the evaluations. In winter the thermal energy produced by the ORC is stored in the thermal energy storage (TES) with a temperature set-point of 70°C. The volume of the storage has a direct impact on the recovery efficiency of the ORC thermal energy, but it is also subject to space constraints in the installation. On the basis of the results from a previous study [51], a size of 1 m<sup>3</sup> per dwelling was considered as a good trade-off. Indeed in [51] a sensitivity analysis of the storage volume was conducted in case of ORC thermal production used only for DHW demand (the thermal energy was assumed given and the plant and building models were not integrated as in this work). The thermal power is used to supply space heating and, when it is not enough, a back-up boiler (Type 122) steps in (a capacity of 25 kW per dwelling was taken). Radiant floor is assumed as distribution system in the building, being the most efficient because of low working temperatures (it was modelled with Type 56 with floor active layer). The inside temperature set-point was set at 20 °C (±0.5 °C) to be maintained 24 h per day with a continuous operation, typical control strategy for such distribution system. The water temperature supplied to the underfloor heating system is regulated on the basis of a linear compensation curve dependent on the outside ambient air temperature ( $T_{air}$ ):

$$T_{supply} = 20 + k_c \cdot (20 - T_{air}) \quad (9)$$

where  $k_c$  is 0.75. The water flow rate is designed to maintain 7 °C as temperature difference between inlet and outlet temperature to the floor and it is 500 kg/h.

The thermal energy produced by the ORC is also retrieved from the TES tank and used for DHW production. A DHW tank of 300 l per dwelling is considered. The daily DHW tap profile is taken from the European standard UNI EN 15316-3, tap profile number 2, because the most representative of the average DHW use in Europe [52]. The back-up boiler is used when the DHW supply temperature is lower than the target value required by the final user.

In summer the TES tank is maintained at 90°C, so that an absorption chiller can be supplied with the stored heat to produce the building cooling demand. A 17 kWc Yazaki Energy System [53] was used (modelled with Type 107), whose condenser is cooled by means of a cooling tower (Type 510)[54]. The same radiant distribution system is considered whilst the water supply temperature is set at 16°C and the flow rate at 800 kg/h. A back-up chiller with an average coefficient of performance of 3 is included to supply the extra cooling demand not satisfied by the absorption chiller.

#### 4. Results and discussion

In this section the results obtained from the simulations are discussed. As previously anticipated they report:

- (i) the micro solar ORC plant performance without building integration (i.e. fixed operating temperatures at the condenser);
- (ii) the micro solar ORC plant performance for the integrated system (plant-building);
- (iii) the building heating system optimization in order to minimize the energy operational costs of the building.

##### 4.1 Micro solar ORC plant performance without building integrations

The performance of the micro solar ORC plant is investigated during a whole year. It is assumed, as often done in literature, that the system can work at given reference conditions at the condenser and in particular all the produced energy can be used by a final user. Firstly the cogeneration configuration is considered, because it is the simplest and corresponds to the prototype configuration of the Innova Microsolar project. In cogeneration mode, all the thermal energy produced by the ORC unit is used to supply space heating and domestic hot water production during the year, thus the return water temperature from the building entering the condenser is assumed at 60°C and the temperature difference equal to 10°C with a fixed flow rate of 0.5 kg/s. In Table 5 the main results of the micro solar ORC plant performance are summarized.

It is possible to notice that, except for the winter months of December and January, the thermal power ( $P_{th,ORC}$ ) is always close to the design value (18 kW), while the average electric power output ( $P_{el,ORC}$ ) is always a bit lower than the design value (2 kW). The yearly electricity production ( $E_{el,ORC}$ ) is about 5400 kWh and the yearly thermal energy ( $E_{th,ORC}$ ) production is about 56330 kWh. Furthermore, as expected, both the thermal and electric energy present bigger production values

during summer time, rather than in winter because the plant works for longer periods (duration of OM2, i.e. plant off, is more than double in winter time as reported in Table 5). However, the electric efficiency of the plant is higher in winter period. This is mainly due to the control strategy of the plant. Indeed, as reported in Table 6, in summer there is more solar radiation and the plant can store surplus energy in the PCM thermal storage and thus work also in operation modes OM5 and OM6 (i.e. the ORC is supplied by the PCM storage or by the PCM storage and the LFR together, respectively). Being the electric efficiency of such configurations much lower than that in the other operation modes, this affects the overall electric efficiency of the system. Furthermore, in mid-season, when the solar radiation increases compared to the winter period, but the system still works in cogeneration mode (i.e. lower condensing temperature), the output thermal and electric power is higher than both winter and summer values.

Table 5. Micro solar ORC plant performance in cogeneration configuration: electric power ( $P_{el,ORC}$ ), thermal power ( $P_{th,ORC}$ ), inlet ( $T_{in,cond}$ ) and outlet ( $T_{out,cond}$ ) condenser temperature, electric energy ( $E_{el,ORC}$ ), thermal energy ( $E_{th,ORC}$ ), electric efficiency ( $\eta_{el,ORC}$ ), thermal efficiency ( $\eta_{th,ORC}$ ).

Month	$P_{el,ORC}$ kW	$P_{th,ORC}$ kW	$T_{in,cond}$ °C	$T_{out,Cond}$ °C	$E_{el,ORC}$ kWh	$E_{th,ORC}$ kWh	$\eta_{el,ORC}$ %	$\eta_{th,ORC}$ %
January	1.59	15.83	60.0	67.6	131.9	1311.3	7.2%	78.0%
February	1.96	18.71	60.0	68.9	266.8	2550.8	7.6%	79.0%
March	1.84	18.64	60.0	68.9	455.9	4613.5	7.0%	81.5%
April	1.74	18.04	60.0	68.6	502.5	5217.3	6.8%	81.8%
May	1.69	17.99	60.0	68.5	614.0	6536.5	6.6%	82.1%
June	1.69	17.93	60.0	68.5	725.3	7693.0	6.6%	82.1%
July	1.64	17.65	60.0	68.4	792.3	8553.7	6.4%	82.3%
August	1.68	17.88	60.0	68.5	689.3	7325.8	6.6%	82.0%
September	1.69	18.05	60.0	68.5	558.5	5947.3	6.6%	82.0%
October	1.88	18.57	60.0	68.9	358.3	3530.5	7.3%	80.7%
November	1.79	17.26	60.0	68.2	191.3	1843.4	7.5%	78.1%
December	1.62	15.91	60.0	67.6	122.5	1206.3	7.3%	77.9%

Table 6. Operation modes duration and efficiency.

Month	OM1 h	OM2 h	OM3 h	OM4 h	OM5 h	OM6 h
January	28.8	515.3	124.3	72.8	2.5	0.0
February	25.5	430.3	86.5	129.5	0.0	0.0
March	22.0	396.7	79.0	200.0	41.7	4.5
April	24.2	310.3	99.2	212.3	63.3	10.5
May	25.2	264.2	99.0	252.0	94.2	9.5
June	16.8	211.8	69.7	294.0	103.7	24.0
July	18.7	192.2	57.0	315.2	131.8	29.2
August	29.7	267.0	51.0	279.3	104.3	12.7
September	17.3	303.0	73.2	230.3	87.7	8.5
October	27.7	435.5	96.7	166.0	16.2	1.8
November	27.8	474.5	121.5	96.0	0.0	0.0

<b>December</b>	20.7	509.0	147.5	66.7	0.0	0.0
$\eta_{el,ORC}$	<b>7.5%</b>			<b>7.6%</b>	<b>3.8%</b>	<b>6.1%</b>
$\eta_{th,ORC}$	<b>79.5%</b>			<b>81.9%</b>	<b>80.2%</b>	<b>78.5%</b>

From these results it is evident that the micro solar ORC plant can produce a huge amount of thermal energy, especially in summer, when the building thermal demand is represented only by domestic hot water if the cogeneration mode is assumed. This means that a lot of dwellings should be coupled to the plant to use all the produced thermal energy [51], while this plant was demonstrated to be particularly suitable for trigeneration applications [55]. For these reasons, the performance of the plant was also evaluated in trigeneration configuration, where during summer months the thermal energy is supplied to the TES at 90°C in order to drive an absorption chiller for space cooling. Table 7 reports the micro solar ORC plant performance during summer period for such configuration.

Table 7. Micro solar ORC plant performance in summer in trigeneration configuration: electric power ( $P_{el,ORC}$ ), thermal power ( $P_{th,ORC}$ ), inlet ( $T_{in,cond}$ ) and outlet ( $T_{out,cond}$ ) condenser temperature, electric energy ( $E_{el,ORC}$ ), thermal energy ( $E_{th,ORC}$ ), electric efficiency ( $\eta_{el,ORC}$ ), thermal efficiency ( $\eta_{th,ORC}$ ).

<b>Month</b>	$P_{el,ORC}$ kW	$P_{th,ORC}$ kW	$T_{in,cond}$ °C	$T_{out,Cond}$ °C	$E_{el,ORC}$ kWh	$E_{th,ORC}$ kWh	$\eta_{el,ORC}$ %	$\eta_{th,ORC}$ %
<b>May</b>	0.96	18.13	80.0	88.7	343.5	6463.0	3.7%	84.7%
<b>June</b>	0.96	18.16	80.0	88.7	405.4	7669.5	3.6%	84.7%
<b>July</b>	0.93	17.93	80.0	88.6	437.5	8466.8	3.5%	84.9%
<b>August</b>	0.94	17.92	80.0	88.6	385.2	7347.5	3.6%	84.6%
<b>September</b>	0.94	18.02	80.0	88.6	311.2	5947.2	3.6%	84.6%

In trigeneration configuration (from May to September), the thermal efficiency is always higher than 84% (against a maximum value of 82% in cogeneration mode), while the higher condensing temperature in summer causes a drop of the electric efficiency of the ORC, which becomes almost half of the winter value. In July the average electric efficiency is 3.5%, whereas in cogeneration mode it reaches 6.4%. As a consequence, the overall electricity production in summer is about 44% less compared to cogeneration configuration, whilst the thermal energy production increases slightly. The electric and thermal efficiency of the ORC are, indeed, strictly connected to the condensation temperature, as shown in Figure 3. It is evident that, given the evaporating temperature, when the condenser inlet temperature increases, the electric efficiency decreases, because it is related to the temperature difference between the evaporator and the condenser. The thermal efficiency, instead, has an opposite trend with the condensing temperature than the electric efficiency and it increases by increasing the condenser temperature.

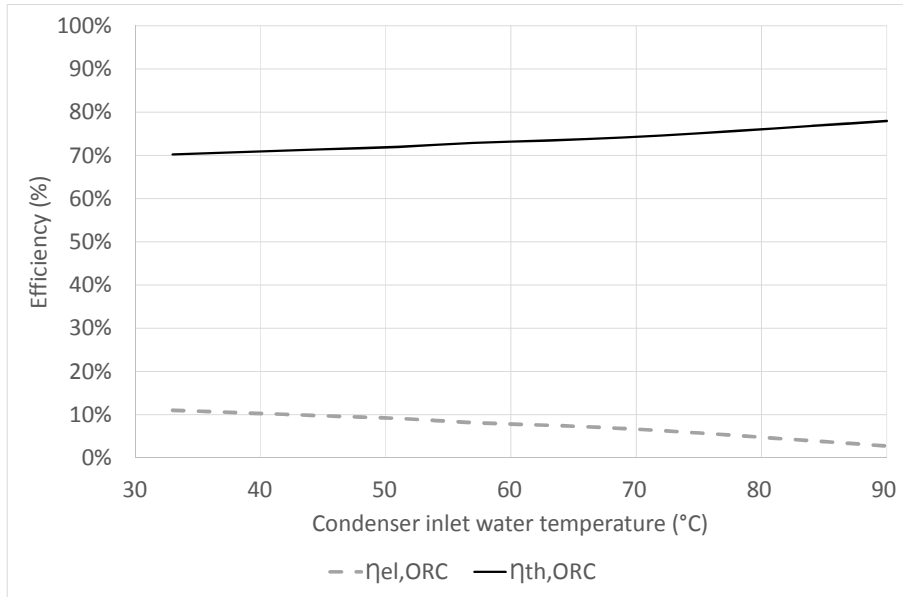


Figure 3. Electric ( $\eta_{el,ORC}$ ) and thermal ( $\eta_{th,ORC}$ ) efficiency of the ORC by varying the condensation temperature (the inlet oil temperature at the evaporator is assumed fixed at 210°C).

#### 4.2 Integrated plant-building system

In this section the micro solar ORC plant is considered coupled to the building described in Section 3.1, whose thermal demand affects the ORC condensation temperature. The trigeneration configuration is selected, because it allows a better exploitation of thermal energy produced in summer. Hence, the thermal energy produced by the ORC is collected in the thermal storage, whose maximum temperature set-point is at 70°C in winter operation and at 90°C in summer operation, delivered with a fixed water flow rate of 0.5 kg/s. With more detail, the operation strategy of the trigeneration unit is as follows: the micro CHP is operated on the basis of solar radiation availability (see conditions in Table 2), while the ORC condensing temperature depends on the user's needs as specified above. The priority is given to the thermal energy production, meaning that the ORC condensing temperature depends on the demand and the electricity is a kind of by product. When there is too much thermal energy produced compared to the demand, an air cooler steps in to cool the water temperature down to 40°C, favouring the electric energy production. Such control strategy allows the system to work a considerable number of working hours (compared to the total number of hours in presence of energy demand) during a year.

In Table 8 the performance of the micro-solar ORC plant when working in the integrated trigeneration configuration is summarized.

Table 8. Micro solar ORC plant performance for the integrated system in trigeneration configuration: electric power ( $P_{el,ORC}$ ), thermal power ( $P_{th,ORC}$ ), inlet ( $T_{in,cond}$ ) and outlet ( $T_{out,cond}$ ) condenser temperature, electric energy ( $E_{el,ORC}$ ), thermal energy ( $E_{th,ORC}$ ), electric efficiency ( $\eta_{el,ORC}$ ), thermal efficiency ( $\eta_{th,ORC}$ ), overall thermal efficiency of the integrated system ( $\eta_{th,int}$ ).

Month	$P_{el,ORC}$ kW	$P_{th,ORC}$ kW	$T_{in,cond}$ °C	$T_{out,Cond}$ °C	$E_{el,ORC}$ kWh	$E_{th,ORC}$ kWh	$\eta_{el,ORC}$ %	$\eta_{th,ORC}$ %	$\eta_{th,int}$ %
January	2.20	15.97	36.9	44.5	195.9	1423.7	9.5%	75.7%	62.2%
February	2.31	18.20	45.8	54.5	331.6	2617.9	9.0%	77.1%	66.4%
March	2.26	18.68	47.0	55.9	554.6	4586.3	8.6%	79.6%	44.6%
April	2.37	18.02	40.5	49.1	654.8	4975.2	9.3%	79.7%	22.9%
May	1.98	18.78	55.6	64.5	594.7	5642.1	7.3%	80.9%	18.9%
June	1.41	18.29	69.2	78.0	551.7	7177.6	5.1%	83.1%	41.0%
July	1.00	17.97	77.0	85.5	460.8	8302.0	3.7%	84.2%	58.7%
August	0.88	18.20	80.9	89.6	346.6	7175.4	3.3%	84.1%	66.5%
September	1.18	18.19	74.1	82.8	368.0	5668.8	4.4%	83.5%	49.0%
October	2.33	18.19	45.4	54.1	453.4	3544.0	8.9%	78	20.1%
November	2.26	17.19	42.4	50.6	253.3	1922.9	9.3%	76.4%	59.5%
December	2.28	16.08	35.6	43.3	182.0	1284.1	9.8%	75.3%	61.4%

The first evident difference with the results shown in the previous section is related to the inlet and outlet water temperatures at the ORC condenser. They are driven by the user thermal demand and are on average lower than the values for the reference condition without building integration. In winter the space heating can, indeed, be supplied with temperature also of 25°C, depending on the outside air ambient temperature (see compensation curve, Eq. 9), while the DHW is mostly demanded at temperatures lower than 45°C. Also in summer the absorption chiller can work with slightly lower activation temperatures. During this season, the ORC thermal energy is used also to cover the DHW demand. Thus the heating supply strategy has a huge impact on the operation and performance of the generation plant, as demonstrated also by comparison with another study available in literature which shows a low energy demand coverage of a solar CHP plant in case of fixed and high supply temperature to the building [ref 26].

The lower condensing temperatures on average allow achieving higher ORC electric efficiency and the electricity production is 26 % higher than the value obtained in the previous section with the trigeneration plant without building integration. Moreover the electric power can even exceed the design value during the winter period. Looking at the ORC thermal efficiency, it does not change considerably in comparison with the trigeneration plant without building integrations. For the integrated trigeneration plant an overall thermal efficiency is also defined:

$$\eta_{th,int} = \frac{P_{th,net}}{P_{in,ORC}} = \frac{P_{th,ORC} - P_{waste} - P_{tank,loss}}{P_{in,ORC}} \quad (10)$$

where  $P_{th,net}$  is the useful thermal power delivered to the building, subtracting the tank thermal losses ( $P_{tank,loss}$ ) and the thermal power dissipated by the air cooler ( $P_{waste}$ ) when the tank is fully

charged and cannot store more energy. As expected the thermal efficiency of the integrated system (ORC plus TES storage) is lower than the ORC thermal efficiency (see Table 8) and the lowest values are related to mid-season, because the thermal demand both for heating and cooling needs is limited. Indeed the reduction of the overall thermal efficiency is mostly due to the waste energy, which reaches about 60% of the ORC output thermal energy in April, May and October. Whereas the tank thermal losses are pretty much constant during the year and account for about 10 % of the ORC thermal production (slightly higher values in winter and slightly lower values in summer, respectively 16 % and 7 %).

From the building point of view, the monthly thermal energy demand breakdown can be seen in Figure 4. The graph shows that there is both a high thermal energy demand for space heating in winter and for space cooling in summer, while in mid-season the heating/cooling need is limited, as already pointed out. As a consequence the waste energy (i.e. the ORC thermal energy that the storage cannot collect because already fully charged and dissipated by the air cooler) is much higher during spring and autumn months, confirming the trend of the overall thermal efficiency above described. The boiler energy integration for DHW production is almost negligible as well as the back-up chiller production. On the contrary, the boiler integration for space heating, especially in January and December, is important.

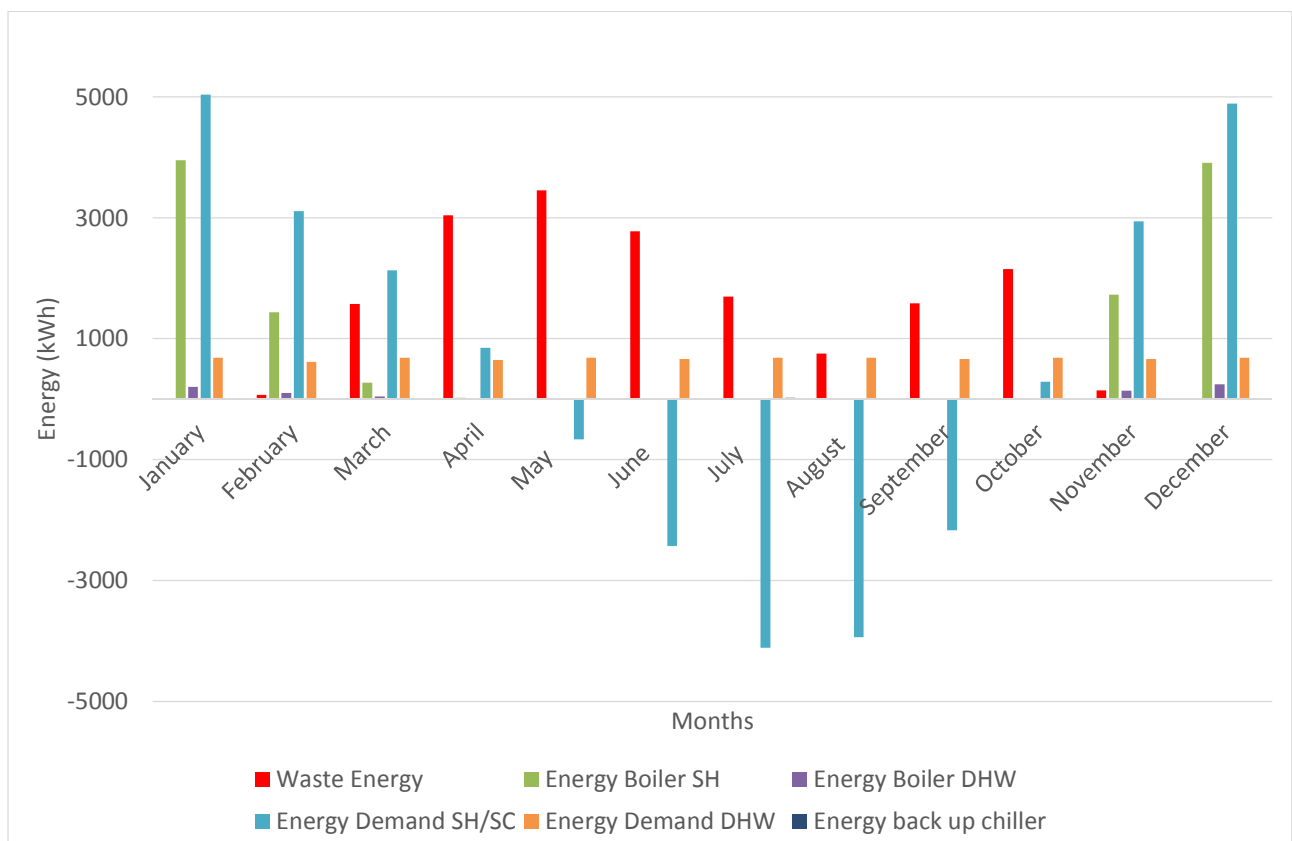


Figure 4. Monthly energy contributions for the considered building: energy demand for space heating (SH) and space cooling (SC), energy demand for domestic hot water (DHW), energy produced by the boiler to integrate the space heating or the domestic hot water, energy produced

by the back-up chiller, energy dissipated by the air-cooler when the storage tank is fully charged (waste energy).

These results are confirmed by the demand coverage factors, defined as the percentage of the corresponding energy demand which is satisfied by the energy produced by the micro-solar ORC without using the back-up generators or the electricity from the grid. They are the space heating thermal energy demand coverage ( $Cov_{SH}$ ), the space cooling thermal energy demand coverage ( $Cov_{SC}$ ), the DHW thermal energy demand coverage ( $Cov_{DHW}$ ), and the total thermal energy demand coverage ( $Cov_{th}$ ) as reported in Table 9. The space cooling is almost completely driven by the ORC thermal energy production, with the exception of few hours during hot peak periods mainly in July. In summer also the DHW demand can be covered for more than 99%, while a relevant share of energy is still wasted, because the production is much bigger than the user request. Some energy is also wasted in mid-season, while other energy needs to be produced by the boiler, because of a shifting in time between demand and production. Thus there are periods when the TES is fully charged and the air cooler has to step in, while in other periods the production is not enough to cover all the users requests. This aspect can be observed in Figure 5a, representing a typical mid-season day: in the morning the boiler steps in to cover the demand because there is not enough energy stored in the tank. When the micro-solar ORC plant starts working, it contributes to supply the building and re-charge the TES. In the evening when the TES reaches the temperature set-point and there is a low thermal energy demand, the ORC thermal energy cannot be used and it is dissipated through the air cooler. In Figure 5b, instead, a winter day is represented. The ORC works a limited number of hours in the afternoon. However the TES is initially partially charged and the heat stored is enough to run the low temperature SH distribution system in the early morning, then the boiler needs also to be switched on. During the considered winter day, the TES can never achieve the temperature set-point (70 °C). Furthermore the boiler has to switch on when the temperature of the DHW tank has a too low temperature level compared to the user's demand. Eventually in summer (Figure 5c), the TES temperature level is higher than in winter in order to run the absorption chiller. It can be observed that the boiler needs sometimes to step in anyway to satisfy an instantaneous high temperature DHW demand. The ORC thermal energy is produced also during night time, thanks to the ORC plant operating strategy, which is driven by the energy stored in the PCM thermal storage.

The electric energy demand coverage ( $Cov_{el}$ ) was evaluated assuming for the electricity demand an average value per dwelling of 3944 kWh/year, derived from available statistical data [35]. The obtained annual electric demand coverage is 31%, while the total energy demand coverage ( $Cov_{tot}$ ) is 73%.

Table 9. Monthly thermal coverage factors: space heating thermal energy demand coverage ( $Cov_{SH}$ ), space cooling thermal energy demand coverage ( $Cov_{SC}$ ), domestic hot water thermal energy demand coverage ( $Cov_{DHW}$ ), total thermal energy demand coverage ( $Cov_{th}$ ) and waste energy.

<b>Month</b>	<b>Waste heat %</b>	<b><math>Cov_{SH}</math> %</b>	<b><math>Cov_{SC}</math> %</b>	<b><math>Cov_{DHW}</math> %</b>	<b><math>Cov_{th}</math> %</b>
<b>January</b>	0.4%	21.5%		70.0%	27.3%
<b>February</b>	2.7%	53.9%		83.9%	58.8%
<b>March</b>	34.3%	87.2%		93.9%	88.8%
<b>April</b>	61.1%	97.6%		99.2%	98.3%
<b>May</b>	61.2%		100.0%	99.8%	99.9%
<b>June</b>	38.7%		99.8%	99.5%	99.7%
<b>July</b>	20.4%		99.4%	99.2%	99.4%
<b>August</b>	10.5%		99.8%	99.4%	99.7%
<b>September</b>	27.9%		100.0%	99.6%	99.9%
<b>October</b>	60.6%	99.9%		99.7%	99.8%
<b>November</b>	7.4%	41.2%		79.0%	48.2%
<b>December</b>	0.4%	20.0%		64.8%	25.5%
<b>tot</b>	31.7%	60.2%	99.8%	90.7%	78.8%

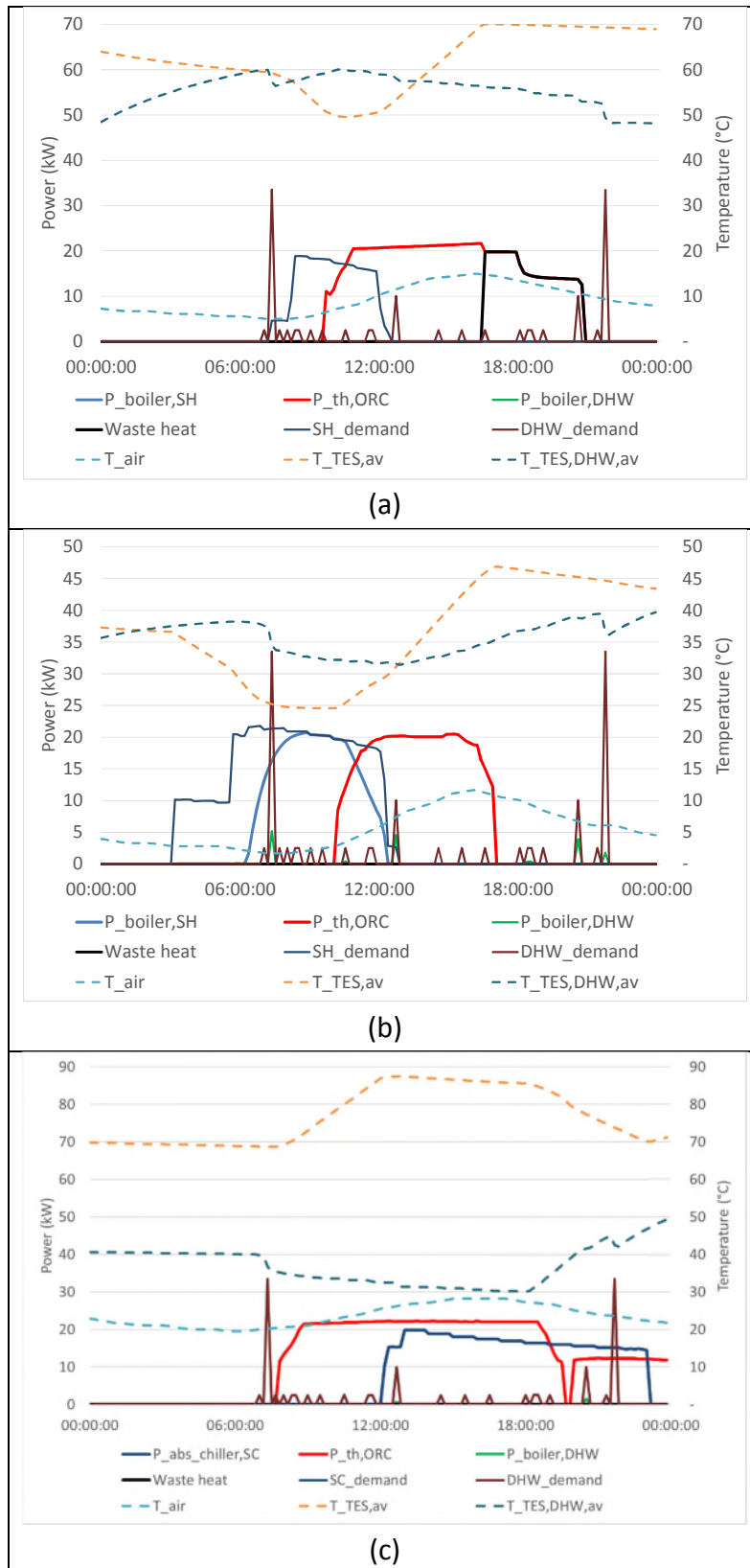


Figure 5. Daily energy flows related to the TES of the integrated system in different representative days: (a) mid-season, (b) winter, (c) summer. The following variables are represented: the boiler power for space heating ( $P_{\text{boiler SH}}$ ) and for domestic hot water ( $P_{\text{boiler DHW}}$ ), the absorption

chiller production ( $P_{abs\_chiller,SC}$ ), the ORC thermal power ( $P_{ORC}$ ), the waste heat, the space heating ( $SH\_demand$ ), the space cooling ( $SC\_demand$ ) and the domestic hot water demand ( $DHW\_demand$ ). The external ambient air temperature ( $T_{air}$ ) and the average temperature of the storage tank ( $T_{TES,av}$ ) and of the DHW tank ( $T_{TES,DHW,av}$ ) are also illustrated.

### 4.3 Optimal building configuration

#### 4.3.1 Influence of design parameters

In this section the influence of the design parameters of the heating/cooling system in the building is investigated in order to minimize energy operational costs. In particular it is investigated if there are different criteria than typical design practice to choose properly their values in an integrated system context. The thermal energy produced by the ORC is considered given and not affected in this case by the user demand itself, so to take into account in the analysis only the effect of the design configuration. The assumed performance for the micro solar ORC system is then that presented in section 4.1 for the plant in trigeneration condition.

The design parameters that can be varied are:

- Volume of the thermal energy storage (TES) between the plant and the building;
- Volume of the DHW storage tank;
- Water flow rate of the heating system;
- Water flow rate of the cooling system;
- Compensation curve of the heating system.

Firstly a sensitivity analysis of the influence of such parameters on the energy operational costs is performed. In Table 10 the considered values of the parameters are reported: a technically feasible lower and higher value of the design value is assumed, in order to look for possible trends in their relationship with costs. The parameters are varied one by one in the dynamic simulation model, while the others are maintained fixed at the design value.

Table 10. Design parameters values used in the sensitivity analysis.

Parameter	Design value	Variations
Volume_TES	4000 l	2000-10000 l
Volume_DHW	1200 l	400-2000 l
Flow rate_SH	500 kg/h	300-1000 kg/h
Flow rate_SC	800 kg/h	500-1000 kg/h
$k_c$	0.75	0.4-1

The operational costs include the electricity costs related to the energy use for the circulation pumps ( $E_{pumps}$ ), for the auxiliaries of the absorption chiller ( $E_{aux}$ ) and for the back-up chiller ( $E_{chiller}$ ) in summer and the natural gas cost for the back-up gas boiler for space heating and DHW (which has an efficiency  $\eta_{boiler}$ ). They are assessed as follows:

$$C_{tot} = (E_{pumps} + E_{aux} + E_{chiller}) \cdot c_{el} + \frac{E_{boiler}}{\eta_{boiler}} \cdot c_{NG} \quad (11)$$

where  $c_{el}$  is the electricity price and  $c_{NG}$  is the natural gas price, whose values are assumed equal to 0.22 €/kWh and 18.52 €/GJ respectively, accordingly to the Spanish market prices [56,57].

In Figure 6 the results of the sensitivity analysis are shown. The cost variation obtained by varying the design parameters is always lower than 2.5%, corresponding to a maximum saving of about 30 €, meaning that their influence is very limited when they are considered separately. Looking at the trends, the operational costs reduction is favoured by a water flow rate reduction for space heating, a water flow rate increase for space cooling, a reduction of the supply water temperature for space heating, an increase of the TES volume and a decrease of the DHW tank volume. In particular, a bigger TES volume allows the storage of more energy, limiting waste energy, and, as a consequence, less extra heating or cooling have to be produced with the back-up generators, while the influence of the DHW tank volume is very limited. Looking at the wasted energy, it drops from 42% to 28% when the TES volume passes from 2000 l to 10000 l. Instead, the lower value of the coefficient  $k_c$  for the compensation curve means that lower temperatures can be conveniently supplied to the radiant floor without any detriment to the internal comfort.

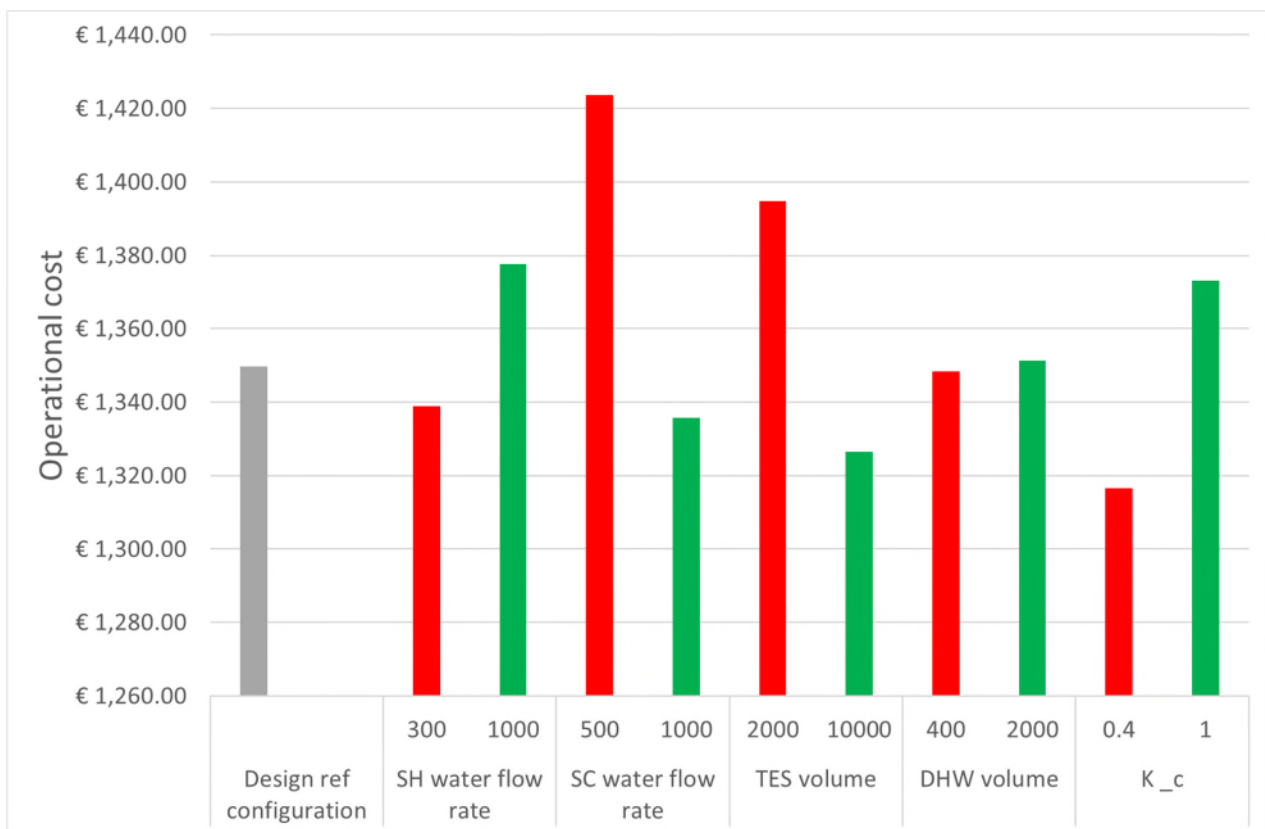


Figure 6. Operational costs variation on the basis of the selected design parameters: space heating and space cooling water flow rates, thermal energy storage volume and domestic hot water volume, compensation curve coefficient ( $k_c$ ).

Eventually an optimization by means of TRNOPT [58] was performed in order to assess the influence of the simultaneous variation of all the considered parameters. TRNOPT is a dedicated TRNSYS

interface for genetic optimization, GenOpt. The algorithm selected for the optimization process is Parametric Runs on a Mesh [58]: this algorithm spans a multi-dimensional grid in the space of the independent parameters, and it evaluates the objective function at each grid point. The parameters considered are the same as those selected for the sensitivity analysis. However in this case they are all varied simultaneously in order to check all the possible combinations of values. The objective function of the optimization analysis is the operational costs minimization (as formulated in Eq. 11). The comfort constraints for the indoor environment and for DHW are considered. The optimal configuration obtained by means of GenOpt optimization provides the best exploitation of the available ORC thermal energy, taking into account the costs for running all the auxiliaries and the natural gas costs when the boiler has to switch on. The optimal trade-off is represented by the following values of the parameters: space heating flow rate 300 kg/h, space cooling flow rate 1000 kg/h, TES volume 10000 l, DHW tank volume 400 l,  $k_c$  value of compensation curve 0.4. The minimum total operational cost is 1230 €, which is about 9 % lower than the cost in the reference design condition.

#### 4.3.2 Influence of final user demand

On the basis of the obtained results, it is evident that a building with 4 dwellings coupled with the considered micro solar ORC system still presents some wasted energy that cannot be recovered to satisfy the final users thermal demand. For this reason it was also evaluated the effect of coupling more dwellings on the wasted energy and final energy use demand coverage. Results are reported in Table 11, where 4, 5, 6 and 10 dwellings are considered. The table shows also primary energy variation ( $PE_{var}$ ) and energy cost variation ( $Cost_{var}$ ) of the proposed micro solar CHP system in comparison with separate generation by means of traditional technologies. The primary energy use by taking the electricity from the grid, by producing thermal energy with a condensing boiler ( $\eta_{boiler}=110\%$ ) and cooling with an electrically driven chiller (coefficient of performance 3) was assessed and compared with the primary energy (PE) use when the micro solar CHP system is introduced (2.5 and 1 were assumed as conversion factors for PE related with electricity and natural gas respectively).

Table 11. Energy coupling performance by varying the dwellings number: space heating thermal energy demand coverage ( $Cov_{SH}$ ), space cooling thermal energy demand coverage ( $Cov_{SC}$ ), domestic hot water thermal energy demand coverage ( $Cov_{DHW}$ ), total thermal energy demand coverage ( $Cov_{th}$ ), waste energy, primary energy variation respect to conventional technologies (PE), percent cost variation ( $Cost_{var}$ ) and absolute cost savings.

Dwellings	Waste heat %	$Cov_{SH}$ %	$Cov_{SC}$ %	$Cov_{DHW}$ %	$Cov_{EI}$ %	$Cov_{Tot}$ %	$PE_{var}$ %	$Cost_{var}$ %	Cost saving €
4	36.7%	35.1%	99.7%	89.0%	22.5%	54.6%	43.3%	42.6%	€ 2,598.96
5	28.5%	31.6%	98.2%	87.4%	18.0%	52.4%	40.0%	39.2%	€ 2,911.18
6	22.7%	28.9%	92.9%	85.9%	15.0%	49.5%	36.7%	35.8%	€ 3,131.23
10	9.9%	20.9%	60.2%	82.3%	9.0%	37.0%	26.3%	25.0%	€ 3,464.23

By increasing the dwellings number from 4 to 10, the wasted energy drops down to 10 %. In turn, the energy share of the back-up generators increases, since the final users demand grows more than the increased amount of energy recovered from the ORC. In particular a limitation is set by the space cooling coverage: the available thermal energy from the ORC in summer (in terms of quantity and temperature) is enough to run an absorption chiller with a cooling capacity of 17 kW. Thus if the number of dwellings is more than 6 the cooling supplied by the absorption chiller becomes much lower than the users cooling demand and the total energy coverage goes down to 50 %. Nevertheless, with 10 dwellings the energy cost reduction, compared to a traditional system, is still about 25 %. The performed analysis shows that the best number of dwellings to be coupled to the considered micro solar CHP depends also on the variable to be optimized (i.e. energy demand coverage, waste energy or costs).

## 5. Conclusions

In this paper the effects of the integration of a novel micro-solar Organic Rankine Cycle system with residential buildings were investigated. In particular, the influence on the ORC electric and thermal performance of the final user dynamic energy demand was analysed by means of an integrated part-building model. Furthermore the incidence of the design parameters of the building heating and cooling system on the energy operational costs was evaluated and an optimal configuration was proposed for the considered case study. Hence, the overall conclusions that can be drawn from the obtained results are:

- the system integration between the micro solar Organic Rankine Cycle plant and the building system cannot be neglected in order to assess properly the Organic Rankine Cycle performance and especially the electric efficiency and energy production. Indeed, the real user demand affects the Organic Rankine Cycle condensing temperature and this aspect has a very huge impact on the Organic Rankine Cycle electric efficiency, while it is limited on the Organic Rankine Cycle thermal production. The possibility of lowering the heating supply temperature has indeed a positive effect on the cogeneration unit and reduces storage thermal losses.
- The high amount of thermal energy produced by similar micro solar combined heat and power systems especially in summer makes such systems particularly suitable for trigeneration configurations, even if this aspect limits the electricity production.
- A bigger storage tank between the plant and the building helps to recover more effectively the thermal energy produced by the Organic Rankine Cycle, limiting wasted energy and energy production from back-up generators. However, space constraints and investment costs have to be taken into account in order to make a proper choice of the thermal energy storage size.
- The proposed micro solar Organic Rankine Cycle plant (2 kW<sub>el</sub>/ 18 kW<sub>th</sub>) is suitable to provide space heating, space cooling and domestic hot water to a number of 100 m<sup>2</sup> dwellings in the region of Lerida ranging from 4 to 6 in order to maintain the overall demand coverage higher than 50 % of the building energy total demand, corresponding to operational cost savings of more than 35 %.

## Acknowledgements

This study has received funding from European Union's Horizon 2020 Research and Innovation programme under grant agreement No 723596 (Innova MicroSolar).

## References

- [1] Buildings - European Commission n.d. <https://ec.europa.eu/energy/en/topics/energy-efficiency/buildings> (accessed December 12, 2018).
- [2] Directive 2004/8/EC of the European Parliament and of the Council of 11 February 2004 on the promotion of cogeneration based on a useful heat demand in the internal energy market and amending Directive 92/42/EEC. 2004.
- [3] Comodi G, Cioccolanti L, Renzi M. Modelling the Italian household sector at the municipal scale: Micro-CHP, renewables and energy efficiency. *Energy* 2014;68. doi:10.1016/j.energy.2014.02.055.
- [4] Bianchi M, De Pascale A, Spina PR. Guidelines for residential micro-CHP systems design. *Appl Energy* 2012. doi:10.1016/j.apenergy.2011.11.023.
- [5] Eurostat, Energy Data, COMBINED HEAT AND POWER GENERATION (CHP) n.d. <https://ec.europa.eu/eurostat/web/energy/data> (accessed January 10, 2019).
- [6] Directive 2009/28/EC of the European Parliament and of the Council of 23 April 2009 on the promotion of the use of energy from renewable sources n.d. <https://eur-lex.europa.eu/legal-content/EN/TXT/HTML/?uri=CELEX:32009L0028&from=ES> (accessed December 12, 2018).
- [7] Murugan S, Horák B. A review of micro combined heat and power systems for residential applications. *Renew Sustain Energy Rev* 2016. doi:10.1016/j.rser.2016.04.064.
- [8] Martinez S, Michaux G, Salagnac P, Bouvier JL. Micro-combined heat and power systems (micro-CHP) based on renewable energy sources. *Energy Convers Manag* 2017. doi:10.1016/j.enconman.2017.10.035.
- [9] Buker MS, Riffat SB. Building integrated solar thermal collectors - A review. *Renew Sustain Energy Rev* 2015;51:327–46. doi:10.1016/j.rser.2015.06.009.
- [10] Tian Z, Perers B, Furbo S, Fan J. Annual measured and simulated thermal performance analysis of a hybrid solar district heating plant with flat plate collectors and parabolic trough collectors in series. *Appl Energy* 2017;205:417–27. doi:10.1016/j.apenergy.2017.07.139.
- [11] Aboelwafa, O; Fateen, S.E.K.; Soliman, A.; Ismail IM. A review on solar Rankine cycles: Working fluids, applications and cycle modifications. *Renew Sustain Energy Rev* 2018;82:868–85.
- [12] Freeman J, Hellgardt K, Markides CN. Working fluid selection and electrical performance optimisation of a domestic solar-ORC combined heat and power system for year-round operation in the UK. *Appl Energy* 2017;186:291–303. doi:10.1016/j.apenergy.2016.04.041.
- [13] Baccioli A, Antonelli M, Desideri U. Dynamic modeling of a solar ORC with compound parabolic collectors: Annual production and comparison with steady-state simulation. *Energy Convers Manag* 2017. doi:10.1016/j.enconman.2017.06.025.
- [14] Manfrida G, Secchi R, Stańczyk K. Modelling and simulation of phase change material latent heat storages applied to a solar-powered Organic Rankine Cycle. *Appl Energy* 2016;179:378–88. doi:10.1016/j.apenergy.2016.06.135.
- [15] Taccani R, Obi JB, De Lucia M, Micheli D, Toniato G. Development and Experimental Characterization of a Small Scale Solar Powered Organic Rankine Cycle (ORC). *Energy Procedia*, vol. 101, 2016, p. 504–11. doi:10.1016/j.egypro.2016.11.064.
- [16] Ramos A, Chatzopoulou MA, Freeman J, Markides CN. Optimisation of a high-efficiency

- solar-driven organic Rankine cycle for applications in the built environment. *Appl Energy* 2018. doi:10.1016/j.apenergy.2018.06.059.
- [17] Calise F, d'Accadia MD, Vicidomini M, Scarpellino M. Design and simulation of a prototype of a small-scale solar CHP system based on evacuated flat-plate solar collectors and Organic Rankine Cycle. *Energy Convers Manag* 2015;90:347–63. doi:10.1016/j.enconman.2014.11.014.
- [18] Fubara TC, Cecelja F, Yang A. Modelling and selection of micro-CHP systems for domestic energy supply: The dimension of network-wide primary energy consumption. *Appl Energy* 2014. doi:10.1016/j.apenergy.2013.09.069.
- [19] ~~Di Marcoberardino, G.; Chiarabaglio, L.; Manzolini, G.; Campanari S. A Techno-economic comparison of micro-cogeneration systems based on polymer electrolyte membrane fuel cell for residential applications. *Appl Energy* 2019;239:692–705.~~
- [20] Rosato A, Sibilio S, Ciampi G. Dynamic performance assessment of a building-integrated cogeneration system for an Italian residential application. *Energy Build* 2013. doi:10.1016/j.enbuild.2013.05.035.
- [21] ~~Rosato A, Sibilio S, Scorpio M. Dynamic performance assessment of a residential building-integrated cogeneration system under different boundary conditions. Part I: Energy analysis. *Energy Convers Manag* 2014;79:731–48. doi:10.1016/j.enconman.2013.10.001.~~
- [22] ~~Sibilio S, Rosato A, Ciampi G, Scorpio M, Akisawa A. Building integrated trigeneration system: Energy, environmental and economic dynamic performance assessment for Italian residential applications. *Renew Sustain Energy Rev* 2017. doi:10.1016/j.rser.2016.02.011.~~
- [23] Fong KF, Lee CK. Investigation of climatic effect on energy performance of trigeneration in building application. *Appl Therm Eng* 2017. doi:10.1016/j.applthermaleng.2017.08.049.
- [24] Romero Rodríguez L, Salmerón Lissén JM, Sánchez Ramos J, Rodríguez Jara EÁ, Álvarez Domínguez S. Analysis of the economic feasibility and reduction of a building's energy consumption and emissions when integrating hybrid solar thermal/PV/micro-CHP systems. *Appl Energy* 2016. doi:10.1016/j.apenergy.2015.12.080.
- [25] G. Yang XQZ. Optimal design and performance analysis of solar hybrid CCHP system considering influence of building type and climate condition. *Energy* 2019;174:647–63. doi:10.1016/j.energy.2019.03.001.
- [26] Martinez S, Michaux G, Salagnac P, Faure J. NUMERICAL INVESTIGATION OF ENERGY POTENTIAL AND PERFORMANCE OF A RESIDENTIAL BUILDING- INTEGRATED SOLAR - CHP SYSTEM 2018:1–20.
- [27] Irene Garcia-Saez, Mendez J, Ortiz C, Loncar D, Becerra JA, Chacartegui R. Energy and economic assessment of solar Organic Rankine Cycle for combined heat and power generation in residential applications. *Renew Energy* 2019;140:461–76. doi:10.1016/j.renene.2019.03.033.
- [28] Zhang Y, Deng S, Zhao L, Lin S, Ni J, Ma M, et al. Optimization and multi-time scale modeling of pilot solar driven polygeneration system based on organic Rankine cycle. *Appl Energy* 2018. doi:10.1016/j.apenergy.2018.03.118.
- [29] Pereira JS, Ribeiro JB, Mendes R, Vaz GC, André JC. ORC based micro-cogeneration systems for residential application - A state of the art review and current challenges. *Renew Sustain Energy Rev* 2018. doi:10.1016/j.rser.2018.04.039.
- [30] Zhixun Wang, Sun S, Lin X, Liu C, Tong N, Sui Q, et al. A remote integrated energy system based on cogeneration of a concentrating solar power plant and buildings with phase change materials. *Energy Co* 2019;187:472–85. doi:10.1016/j.enconman.2019.02.094.
- [31] Arteconi A, Del Zotto L, Tascioni R, Mahkamov K, Underwood C, Cabeza L, et al. Multi-

Country Analysis on Energy Savings in Buildings by Means of a Micro-Solar Organic Rankine Cycle System: A Simulation Study. *Environments* 2018;5:119. doi:10.3390/environments5110119.

- [32] Cioccolanti L, Tascioni R, Arteconi A. Mathematical modelling of operation modes and performance evaluation of an innovative small-scale concentrated solar organic Rankine cycle plant. *Appl Energy* 2018;221:464–76. doi:10.1016/j.apenergy.2018.03.189.
- [33] Innova-Microsolar n.d. <http://innova-microsolar.eu/> (accessed November 3, 2017).
- [34] Northumbria University | Newcastle upon Tyne | Study in the Best Student City n.d. <https://www.northumbria.ac.uk/> (accessed December 28, 2017).
- [35] Electricity use per household | Electricity Consumption Efficiency| WEC n.d. <https://wec-indicators.enerdata.net/household-electricity-use.html> (accessed January 11, 2019).
- [36] TRNSYS : Transient System Simulation Tool n.d. <http://www.trnsys.com/> (accessed November 14, 2017).
- [37] MATLAB - MathWorks n.d. <https://www.mathworks.com/products/matlab.html> (accessed November 14, 2017).
- [38] EnergyPlus - Weather Data Sources n.d. <https://energyplus.net/weather/sources> (accessed January 11, 2019).
- [39] Elianto S.R.L - Home n.d. <http://www.eliantocsp.it/index.php/en/> (accessed November 14, 2017).
- [40] Enogia | Home n.d. <http://www.enogia.com/> (accessed November 14, 2017).
- [41] 3M™ Novec™ 649 Engineered Fluid n.d.
- [42] Thermacore n.d. <http://www.thermacore-europe.com/> (accessed December 28, 2017).
- [43] Maldonado J, Fullana-Puig M, Martín M, Solé A, Fernández Á, de Gracia A, et al. Phase Change Material Selection for Thermal Energy Storage at High Temperature Range between 210 °C and 270 °C. *Energies* 2018;11:861. doi:10.3390/en11040861.
- [44] Serrano-López R, Fradera J, Cuesta-López S. Molten salts database for energy applications. *Chem Eng Process* 2013. doi:10.1016/j.cep.2013.07.008.
- [45] Gantenbein P, Jaenig D, Kerskes H, Van Essen M. Final report of Subtask B “Chemical and Sorption Storage”; The overview A Report of IEA Solar Heating and Cooling programme -Task 32 Advanced storage concepts for solar and low energy buildings Report B7 of Subtask B 2008.
- [46] S.TRA.TE.G.I.E. srl n.d. <http://www.strategiesrl.com/eng/Default.aspx> (accessed December 29, 2017).
- [47] Cioccolanti L, Tascioni R, Bocci E, Villarini M. Parametric analysis of a solar Organic Rankine Cycle trigeneration system for residential applications. *Energy Convers Manag* 2018;163. doi:10.1016/j.enconman.2018.02.043.
- [48] Coma, J.; Maldonado, J.M.; De Gracia, A.; Gimbernat, T.; Botargues, T.; Cabeza LF. Benchmarking of Energy Storage, Demand of Residential Buildings. *Proc. 14th Int. Conf. Energy (Enerstock 2018)*, Adana, Turkey: n.d.
- [49] Atanasiu B, Maio J, Staniaszek D. Overview of the EU-27 building policies and programmes-WP5 ENTRANZE. n.d.
- [50] EU Buildings Database - European Commission n.d. <https://ec.europa.eu/energy/en/eu-buildings-database> (accessed January 11, 2019).
- [51] Arteconi A, Del L, Tascioni R, Mahkamov K, Cabeza LF, Gracia A De, et al. Simulation analysis of an innovative micro-solar 2kWe Organic Rankine Cycle plant coupled with a multi-apartments building for domestic hot water supply. *Energy Procedia*, vol. 158, 2019, p. 2225–30. doi:10.1016/j.egypro.2019.01.168.

- [52] prEN 15316-3-1, Heating systems in buildings — Method for calculation of system energy requirements and system efficiencies — Part 3-1 Domestic hot water systems, characterisation of needs (tapping requirements). 2006.
- [53] Yazaki Energ Systems, Inc. n.d. <http://www.yazakienergy.com/> (accessed November 7, 2017).
- [54] Thermac, Air handling n.d. <http://www.thermac.it/> (accessed January 11, 2019).
- [55] Villarini M, Tascioni R, Bocci E. Modelling of two small-scale solar Organic Rankine Cycle trigeneration systems and comparison of their thermodynamic performance. 13th Conf. Sustainable Dev. Energy, Water an Environ. Syst., Palermo, Italy: 2018, p. 1–12.
- [56] Electricity price statistics - Statistics Explained n.d. [http://ec.europa.eu/eurostat/statistics-explained/index.php/Electricity\\_price\\_statistics](http://ec.europa.eu/eurostat/statistics-explained/index.php/Electricity_price_statistics) (accessed March 5, 2018).
- [57] Natural gas price statistics - Statistics Explained n.d. [http://ec.europa.eu/eurostat/statistics-explained/index.php/Natural\\_gas\\_price\\_statistics](http://ec.europa.eu/eurostat/statistics-explained/index.php/Natural_gas_price_statistics) (accessed March 5, 2018).
- [58] Wetter M, Gov M. GenOpt manual. 2016.